Postprint of: Mul M., Lamęcki A., Gómez-García R., Mrozowski M., Inverse Nonlinear Eigenvalue Problem Framework for the Synthesis of Coupled-Resonator Filters With Nonresonant Nodes and Arbitrary Frequency-Variant Reactive Couplings, IEEE TRANSACTIONS ON MICROWAVE THEORY AND TECHNIQUES (2021), DOI: 10.1109/TMTT.2021.3119288

Inverse Nonlinear Eigenvalue Problem Framework for the Synthesis of Coupled-Resonator Filters With Nonresonant Nodes and Arbitrary Frequency-Variant Reactive Couplings

Martyna Mul, Adam Lamecki , *Senior Member, IEEE*, Roberto Gómez-García , *Senior Member, IEEE*, and Michal Mrozowski , *Fellow, IEEE*

***Abstract*— A novel, general circuit-level description of coupled-resonator microwave filters is introduced in this article. Unlike well-established coupling-matrix models based on frequency-invariant couplings or linear frequency-variant couplings (LFVCs), a model with arbitrary reactive frequency-variant coupling (AFVC) networks is proposed. The engineered formulation is more general than prior-art ones—with the only restriction that the coupling network is a reactive-type two-port circuit—and can be treated as an extension of previous synthesis models since constant or linear couplings are special cases of arbitrary frequency dependence. The suggested model is fully general, which allows for AFVCs with highly nonlinear (even singular) characteristics, loaded or unloaded nonresonating nodes (NRNs), frequency-dependent source–load coupling, multiple frequency-variant cross couplings, and/or multiple dispersive couplings for connecting the source and load to the filter network. The model is accompanied by a powerful synthesis technique that is based on the zeros and poles of the admittance or scattering parameters and the eigenvalues of properly defined eigenproblems. In the most general case, the zeros and poles of the admittance or scattering parameters are related to solutions of nonlinear eigenvalue problems. The synthesis is defined as an inverse nonlinear eigenvalue problem (INEVP) where the matrix is constructed from three sets of eigenvalues. This is accomplished by optimization using an iterative nonlinear least-squares solver with excellent convergence property. Finally, the third- and fifth-order examples of bandpass filter topologies involving AFVCs are shown, and the experimental validation of the proposed theory is presented through the manufacturing and characterization of a microstrip filter prototype with transmission zeros (TZs).**

***Index Terms*— Coupling matrix, microwave filters, synthesis.**

Manuscript received July 16, 2021; revised August 23, 2021; accepted August 25, 2021. This work was supported by the Polish National Science Centre under Contract UMO-2019/33/B/ST7/00889. *(Corresponding author: Michal Mrozowski.)*

Martyna Mul, Adam Lamecki, and Michal Mrozowski are with the Faculty of Electronics, Telecommunications and Informatics, Gdańsk University of Technology, 80-233 Gdańsk, Poland (e-mail: martyna.mul@pg.edu.pl; adam.lamecki@ieee.org; m.mrozowski@ieee.org).

Roberto Gómez-García is with the Department of Signal Theory and Communications, Polytechnic School, University of Alcalá, 28871 Alcalá de Henares, Spain (e-mail: roberto.gomez.garcia@ieee.org).

Color versions of one or more figures in this article are available at https://doi.org/10.1109/TMTT.2021.3119288.

Digital Object Identifier 10.1109/TMTT.2021.3119288

I. Introduction

COUPLED-RESONATOR bandpass filters are one of the fundamental microwave components in RF front-end chains to preselect the desired RF signals and suppress unwanted out-of-band interfering signals and noise. While different design approaches to synthesize bandpass filters have become well established during the years, the coupling-matrix formulation has acquired a paramount importance among researchers since its inception [1]. This modeling framework is based on a lumped-element circuit representation of the filter, which reflects the topology of its resonator network and the strength and nature of the interactions between its resonating elements. Conventional techniques for coupling-matrix synthesis generally assume that the inter-resonator coupling structures, also referred to as impedance or admittance inverters, do not vary with frequency [2]–[5]. As a result, the accuracy of this model to fairly represent the overall response of the filtering device is mostly restricted to narrow-to-moderate-bandwidth specifications. To partially circumvent this limitation by considering specific frequency-variation profiles for couplings, a new broadband model for the coupling matrix in the passband domain was introduced in [6] that results in coupling elements to be inversely proportional to frequency. In [7], a combination of frequency-dependent inductive or capacitive couplings was considered for higher modeling accuracy in wideband spectral intervals. In both cases, the goal was to broaden the frequency range of the coupling-matrix representation of a filter and to be able to place the transmission zeros (TZs) at arbitrary positions, including a finite number of TZs at the zero and infinity frequencies. However, as already demonstrated during the first decade of this century, dispersion—i.e., frequency-dependence—in couplings can be conveniently exploited even for narrowband bandpass filters in inline [8]–[11] or triplet [12] topologies to generate additional TZs without significantly increasing the complexity of the associated inter-resonator coupling arrangement.

Since the realization of high-selectivity bandpass filtering actions in compact circuits with simple inter-resonator coupling schemes is a desired feature, a new synthesis technique

aimed at filtering networks with arbitrarily connected dispersively cross-coupled resonators was proposed in [13]. An advanced version of this synthesis method that includes resonant-type source–load coupling to produce $n + 1$ TZs in the nth-order bandpass filters was subsequently suggested in [14] and then refined in [15] to also account for the resonator-detuning effect due to the nonideal dispersive couplings. The three variants of this technique share, as common principle, the fact that the zeros and poles in a cross-coupled filter with linear frequency-variant coupling (LFVC) or inverters (LFVIs) in the low-pass prototype domain are the roots of the characteristic equation for the generalized eigenvalue problem. On the other hand, new direct coupling-matrix synthesis techniques for inline and cascaded topologies with LFVCs have been lately developed, such as those in [16] and [17], respectively.

Although linear frequency variation in couplings is often sufficient to describe the filter behavior accurately, couplings may exhibit more complex frequency-dependent patterns, which can be employed to further increase selectivity. Examples of such generalized coupling networks for different RF technologies encompass coupling elements in the form of an iris with complex geometry [18] and an internal bypass metallic loop structure [19] in the case of waveguide filters or even alternative types of source–load coupling with additional transmission-line and waveguide sections in the input/output accesses for planar and 3-D implementations. The latter case is especially suitable to further augment the number of produced TZs due to the transversal signal-interference phenomenon so that increased attenuation levels can be achieved in multiples regions of the stopband range [20]–[23]. However, previously mentioned coupling-matrix synthesis approaches are not fully applicable to such more general filtering configurations.

In order to provide a systematic design methodology for a much-broader variety of filtering structures, a novel coupling-matrix model and synthesis technique, which allows for arbitrary frequency variation of inverters, are reported in this article. Furthermore, since the inter-resonator couplings cannot be implemented as ideal inverters—i.e., two-port networks with admittance/impedance matrices having zero diagonal elements—while detuning the resonators at the same time, this loading effect is directly considered here during the synthesis process by additionally allowing for it to be frequency-dependent. Finally, in order to increase flexibility in terms of distinct classes of filter networks that can be synthesized by means of the devised filter synthesis procedure, the inclusion of nonresonating nodes (NRNs) is also considered. The frequency profile of the arbitrary reactive frequency-variant coupling (AFVC) can be highly nonlinear and even show singularities that generate poles. The only restriction is that the coupling has to be a linear reciprocal lossless lumped- or distributed-element two-port network with the Foster representation given by [24]

$$\mathbf{Z}(\omega) = \frac{\mathbf{A}_0}{j\omega} + \sum_{i=1}^{\infty} \frac{j\omega \mathbf{A}_i}{\omega_i^2 - \omega^2} \tag{1}$$

where $\mathbf{A}_i$ $(i = 0, 1, \ldots)$ are 2×2, real-valued, frequency-independent, rank-1 matrices, and ω_i are poles. This ensures that the AFVC describes a physically realizable circuit. To the best of the authors' knowledge, no coupling-matrix-based filter model and synthesis technique of such level of generality has been proposed in the technical literature to date. Note that existing models with constant couplings or LFVCs may be regarded as a zeroth- or first-order approximations of the Foster representation.

The organization of the rest of this article is as follows. In Section II, the theoretical foundations of the proposed coupling-matrix synthesis methodology formulated as an inverse eigenvalue problem are presented. In Section III, a new filter model is introduced. Next, the step-by-step synthesis procedure for filter networks with nonideal AFVCs or inverters (AFVIs), which can also include NRNs to increase the variety of affordable filtering topologies, is described. Specific types of AFVCs particularized in transmission-line realizations are shown in Section IV, which are then used in Section V for several theoretical examples of equiripple-type third- and fifth-order bandpass filters with TZs derived from the engineered coupling-matrix synthesis method. In Section VI, the experimental results of a built proof-of-concept microstrip prototype associated with one of the third-order filter examples previously synthesized are provided. Section VII gives a brief discussion of limitations of the proposed approach. Finally, a summary and the main concluding remarks of this work are set out in Section VIII.

II. Synthesis of a Coupling Matrix as an Inverse Eigenvalue Problem

A. Theoretical Foundations

The fundamental core of the proposed synthesis technique is the relationship existing between the zeros and poles of the short-circuit admittance or scattering parameters of the filter network and the eigenvalues of the coupling matrix and its two principal submatrices. Therefore, a few basic preliminaries related to various categories of eigenproblems will be given first. In the simplest case of a standard eigenvalue problem with one matrix $\mathbf{A}$, nontrivial solutions are sought of a matrix equation

$$(\mathbf{A} - \lambda \mathbf{I})\mathbf{x} = 0 \tag{2}$$

where $\mathbf{I}$ is the identity matrix and λ is a scalar that is called eigenvalue. This equation has nonzero solution(s) if the determinant of the matrix $(\mathbf{A} - \lambda \mathbf{I})$ is zero. Therefore, the eigenvalues are the roots of the characteristic equation $\det(\mathbf{A} - \lambda \mathbf{I}) = 0$. Analogously, the generalized eigenvalue problem with a pair of matrices $(\mathbf{A}, \mathbf{B})$ is defined as

$$(\mathbf{A} - \lambda \mathbf{B})\mathbf{x} = 0 \tag{3}$$

so that the eigenvalues are the roots of

$$\det(\mathbf{A} - \lambda \mathbf{B}) = 0. \tag{4}$$

This can be made even more general by considering a parameter-dependent matrix $\mathbf{A}(\lambda)$ and the nonzero solutions of equation $\mathbf{A}(\lambda)\mathbf{x} = 0$. This equation defines a nonlinear

matrix eigenvalue problem. Again, the eigenvalues are the roots of the characteristic equation $\det \mathbf{A}(\lambda) = 0$. To find the eigenvalues for a given matrix, numerical procedures have to be applied. For standard and generalized eigenproblems, the QR and QZ algorithms are recommended [25]. For a nonlinear problem, the characteristic equation can be either solved directly by using a root-finding algorithm [26]–[28] or indirectly by applying a specialized technique for parameter-dependent matrices [29], [30].

After these preliminary remarks, the relation of various categories of eigenvalue problems to the synthesis of coupled-resonator filters can be explained. To start with, let it be considered the conventional circuit description of a bandpass filter consisting of a two-port network. For such filter circuit, Kirchhoff's voltage law reads as follows:

$$\mathbf{Z}_n(\omega)\mathbf{i} = \mathbf{e} \tag{5}$$

where $\mathbf{Z}_n(\omega)$ is a frequency-dependent impedance matrix for the network, $\mathbf{i}$ is a vector of loop currents, and $\mathbf{e}$ is the voltage source vector. In a conventional coupled-resonator synthesis technique, Kirchhoff's equations are expressed in the low-pass prototype domain Ω as follows:

$$\Omega = \frac{1}{\Delta}\left(\frac{\omega}{\omega_0} - \frac{\omega_0}{\omega}\right) \tag{6}$$

where ω_0 is the center frequency of the bandpass filter and Δ is its fractional bandwidth. Using this frequency transformation, the following formula is obtained for the entire network:

$$[\mathbf{R} + j(\mathbf{M}_c + \Omega\mathbf{I})]\mathbf{i} = \mathbf{e} \tag{7}$$

where $\mathbf{M_c}$ is the (symmetric) coupling matrix, $\mathbf{R}$ is the matrix corresponding to the source and load resistances (this matrix is zero except for the first and last element on the main diagonal that take the value of the internal resistance of the source and load, respectively), and $\mathbf{I}$ is the identity matrix. In this work, it is assumed that the coupling matrix is symmetric, but nonsymmetric matrices, such as in [31], can also be considered. The reactive part of the network can be characterized by the short-circuit admittance parameters [5]. For instance, y_{11}^c is given by

$$y_{11}^c = -j[\mathbf{M}_c + \Omega\mathbf{I}]_{11}^{-1} = -j\frac{\det[\mathbf{M_c'} + \Omega\mathbf{I'}]}{\det[\mathbf{M_c} + \Omega\mathbf{I}]} \tag{8}$$

where the prime symbol is used to denote the matrices with the first row and first column deleted. Such matrix will be called lower principal submatix. A similar expression can be formulated for the short-circuit output admittance y_{22}^c except that an upper principal submatrix, obtained by deleting the last row and column of the matrix $\mathbf{M_c}$, is used instead in the numerator. For the transadmittance parameter y_{21}^c, an analogous formula that involves a submatrix obtained from $\mathbf{M_c}$ by deleting the first column and last row (upper right principal submatrix) can be derived. Referring to (4), it is then evident that the expression in the numerator and denominator for all admittance parameters is the characteristic equation for finding the eigenvalues. Hence, the poles of the admittance parameters are the eigenvalues of the coupling matrix $\mathbf{M_c}$, while the zeros of the short-circuit admittance parameters are the eigenvalues of its appropriate principal submatrices. Equation (8) is valid for a traditional category of filters, in which the coupling elements are frequency-invariant. However, this assumption can be relaxed by allowing for linear frequency variation of the inverters (in the prototype domain) so that $\mathbf{M_c} = \mathbf{M_0} + \Omega\mathbf{M_1}$. In such case, the input short-circuit admittance of the reactive part is as follows:

$$y_{11}^c = -j[\mathbf{M_0} + \Omega\mathbf{M_1}]_{11}^{-1} = -j\frac{\det\left[\mathbf{M_0'} + \Omega\mathbf{M_1'}\right]}{\det[\mathbf{M_0} + \Omega\mathbf{M_1}]}. \tag{9}$$

Again, the prime symbol is used to refer to the lower principal submatrix of a matrix. The expressions for the remaining short-circuit admittance parameters have a similar form. As a result, the poles of the admittance parameters are eigenvalues of the symmetric matrix pencil $(\mathbf{M_0}, \mathbf{M_1})$, while the zeros of the short-circuit admittance parameters are eigenvalues of pencils obtained from the pair $(\mathbf{M_0}, \mathbf{M_1})$ by deleting an appropriate row and column. At this point, an observation can be made related to the equivalence of filters with constant couplings and filters with LFVCs. A symmetric generalized eigenvalue problem can be transformed to a standard one as follows:

$$(\mathbf{A} - \lambda\mathbf{B})\mathbf{x} = \left(\mathbf{B}^{1/2}\mathbf{A}\mathbf{B}^{1/2} - \lambda\mathbf{I}\right)\mathbf{x} = 0. \tag{10}$$

Obviously, the structure (nonzero pattern) of $\mathbf{B}^{1/2}\mathbf{A}\mathbf{B}^{1/2}$ is different from the structure of the pencil. From the filter synthesis perspective, this equivalently means that every filter network with LFVCs can be implemented as a filter with constant couplings, albeit with a different coupling scheme, as observed also in [8].

The matrix eigenvalue problems considered above arise from the expressions for the short-circuit admittance parameters derived from the Kirchhoff equations. These equations are quite general, so nothing prevents this study from going one step further, and assume that the inverters in the coupling matrix exhibit more-general frequency dependence. For this situation, all the elements of the reactance matrix will be frequency-variant. As a result, the expression for the short-circuit input admittance of the reactive part adopts the following form:

$$y_{11}^c = -j[\mathbf{X}(\Omega)]_{11}^{-1} = -j\frac{\det\left[\mathbf{X}'(\Omega)\right]}{\det[\mathbf{X}(\Omega)]}. \tag{11}$$

As in the previous two cases, the formula in the numerator and denominator is the characteristic equation, this time for nonlinear eigenvalue problems involving the entire reactance matrix $\mathbf{X}(\Omega)$ and lower principal submatrix $\mathbf{X}'(\Omega)$.

It is obvious that, regardless of the assumed frequency dependence of the reactance matrix, the zeros and poles of the admittance parameters are nothing else but the eigenvalues of properly defined matrices or matrix pencils. Since the zeros and poles of the short-circuit admittance parameters for a given filter configuration can be derived analytically from the filtering function [5], the coupling-matrix synthesis is in fact an inverse matrix eigenvalue problem. This problem, in linear algebra, refers to the construction of a matrix with the prescribed structure from its eigenvalues.

Based on the observations made so far, this section concludes with the definition of the coupling-matrix synthesis

in terms of inverse eigenvalue problem (IEVP). Note that depending on the frequency behavior of the inverters, the IEVP may be of the standard, the generalized or, in the most general form, of the nonlinear type.

Definition 1 (Coupling-Matrix Synthesis as an IEVP): Given the three known rational functions y_{11}, y_{21}, and y_{22} corresponding to the desired short-circuit admittance parameters of a filter and the intended coupling-routing scheme, the coupling-matrix synthesis as an IEVP can be set as finding a symmetric reactance matrix $\mathbf{X}(\Omega)$ with the structure (i.e., locations of the nonzero elements) determined by the coupling-routing scheme such that it satisfies the following conditions.

1) Its eigenvalues are the poles of y_{11} and y_{22}.
2) The eigenvalues of its lower principal submatrix are the zeros of y_{11}.
3) The eigenvalues of its upper right principal submatrix are the zeros of y_{21}.
4) The eigenvalues of its upper principal submatrix are the zeros of y_{22}.

Some additional remarks to be considered are given as follows.

Remark 1: To synthesize the reactive part of a lossless filtering network, only two rational functions are needed. However, for lossy filters, synthesis scenarios based on three sets have to be used [32].

Remark 2: For frequency-invariant inverters (FIIs) and dispersive inverters with linear frequency variation, the reactance matrix $\mathbf{X}(\Omega)$ is given by $\mathbf{M_c}+\Omega\mathbf{I}$ and $\mathbf{M_0}+\Omega\mathbf{M_1}$, respectively, and the eigenvalues of $\mathbf{X}(\Omega)$ are simply the eigenvalues of the matrix $\mathbf{M_c}$ or matrix pencil $(\mathbf{M_0}, \mathbf{M_1})$.

Remark 3: For a large number of coupling schemes with FIIs, the solution to the IEVP involving the matrix $\mathbf{M_c}$ can be found directly by a series of eigenvalue-preserving similarity transformations applied to the transversal matrix, which can be found analytically [5].

Remark 4: A solution of the IEVP for all three categories of frequency variation of inverters considered here can be formulated in terms of the optimization problem. The details will be presented in Section III.

Remark 5: In the IEVP framework, the synthesis problem can also be solved in the bandpass domain. In this case, only the nonlinear variant is applicable.

Remark 6: In contrast to standard and generalized eigenvalue problems, the number of eigenvalues in a nonlinear eigenvalue problem can be greater than the size of the matrix. This is especially true when the matrix elements are periodic-type functions. In this case, the synthesis gives rise to a network with a response that properly matches the filter specification only within a certain bandwidth.

B. Alternative Formulations

The formulation presented above based on short-circuit admittance parameters is not directly applicable to more complex coupling schemes, such as those of filters involving multiple dispersive couplings for connecting the source and load as well as direct, possibly resonant-type, source–load connections. One possible alternative—more-general—formulation for the synthesis as an INEVP can be derived by considering the relationship that links the coupling matrix and the scattering parameters. For the frequency-invariant model, the following formula is obtained:

$$S_{11}(\Omega) - 1 = 2jR_s \frac{\det\left(\mathbf{M}_\mathbf{c}' - j\mathbf{R}' + \Omega\mathbf{I}'\right)}{\det(\mathbf{M_c} - j\mathbf{R} + \Omega\mathbf{I})}. \tag{12}$$

In the above expression, it is immediate to recognize the characteristic equations for the eigenvalues of complex matrices $\mathbf{M}_\mathbf{c}' - j\mathbf{R}'$ and $\mathbf{M}_c - j\mathbf{R}$ for the numerator and denominator, respectively. Allowing for the inverters to exhibit an arbitrary frequency-variation profile, a generalized equivalent version of (12) can be written as follows:

$$S_{11}(\Omega) - 1 = 2jR_s \frac{\det\left(\mathbf{X}'(\Omega) - j\mathbf{R}'\right)}{\det(\mathbf{X}(\Omega) - j\mathbf{R})}. \tag{13}$$

Analogous expressions, but with different principal submatrices in the numerator, arise for $S_{22}(\Omega) - 1$ and $S_{21}(\Omega)$. Specifically, the expression for $S_{22}(\Omega) - 1$ involves the upper submatrix of $\mathbf{X}(\Omega) - j\mathbf{R}$, whereas the one for $S_{21}(\Omega)$ uses the upper right submatrix.

It is now evident that the synthesis can be considered in terms of the zeros and poles of expressions related to the scattering parameters and solved via an INEVP involving an alternative set of roots of the characteristic equations for the numerator and denominator. The reference roots can be taken from the formulas defining the scattering parameters in terms of polynomials generated by the filtering function [5]. Alternatively, the reference poles and zeros for the construction of the coupling matrix with AFVC can be determined from the characteristic equations for the numerator and denominator of the filter with frequency-invariant couplings. This links the approach proposed in this article with synthesis techniques developed in the past for particular configurations, such as the transversal topology that allows for fully canonical filters [5], resonant-type source–load coupling [14], or frequency-dependent m_{SS} and m_{LL} [33]. A filter with a desired characteristic can be synthesized with frequency-invariant couplings and the resulting coupling matrix can be then substituted into (25), providing the reference zeros and poles that are needed in the INEVP—which is solved for the target coupling topology and frequency-variant inverters.

Finally, it should be remarked upon that, for some cases, the reference eigenvalues may also be obtained directly by computing three sets of eigenvalues of reference coupling matrices with FIIs [34].

III. Filters With Nonideal Arbitrary Frequency-Variant Inverts and Nonresonating Nodes

For the sake of generality, a filter network consisting of N reactances $jX_i(\omega)$ $(i = 1, 2, \ldots, N)$ that are mutually coupled through inverters is considered. The network is connected to the source and load by means of input and output inverters. This gives rise to an $N + 2$ network—i.e., N in-series reactances plus the source and load—as shown in Fig. 1.

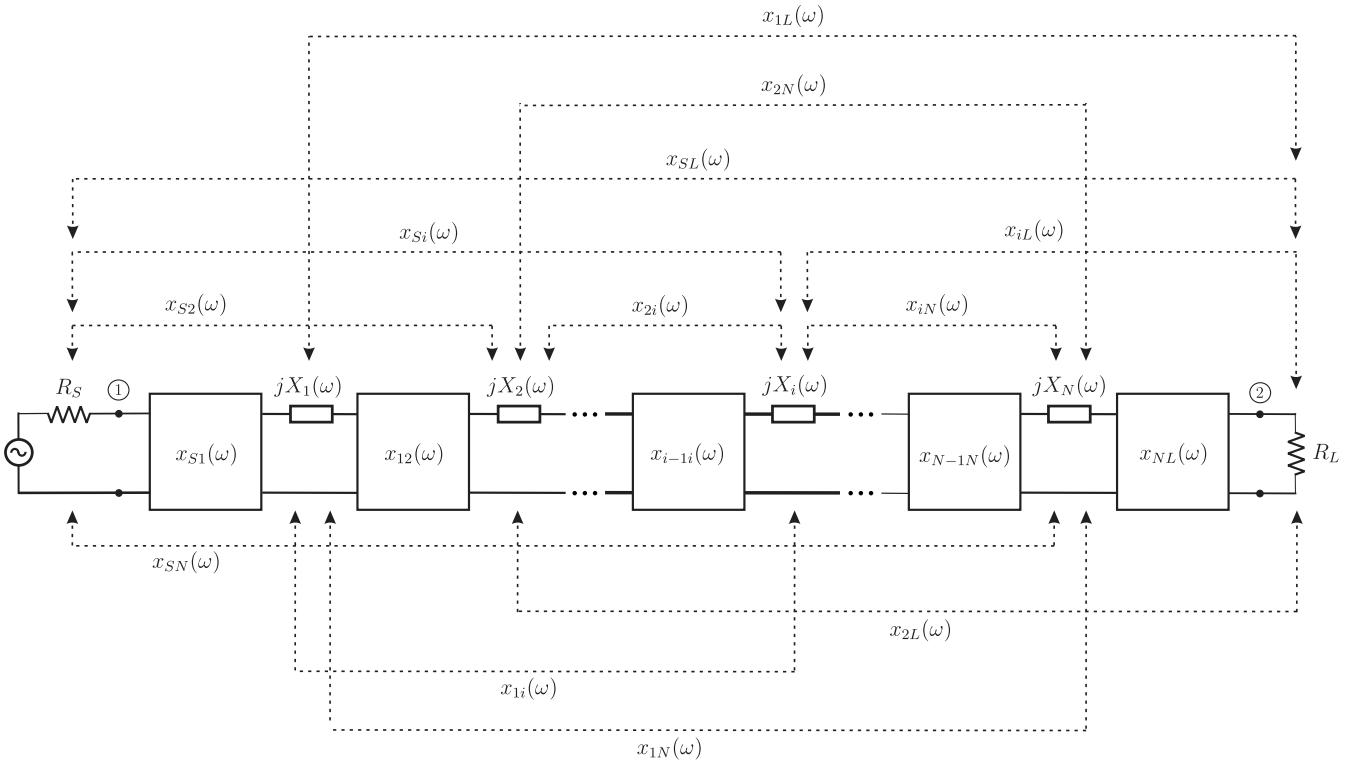

Fig. 1. $N+2$ network with multicoupled series reactances. All the elements in the network are assumed to be frequency-variant.

The series reactances in the filter network, which are frequency-dependent, can be either resonators or nonresonating elements. In particular, the ith reactance can be mathematically expressed as follows:

$$jX_i = j\chi_i(\omega/\omega_{i1} - \omega_{i2}/\omega). \tag{14}$$

This general formula covers various possibilities for a filter network represented by a coupling diagram with different types of nodes as follows.

1) Resonator—when $\omega_{i1} = \omega_{i2} = \omega_i$ where ω_i is the resonant frequency and χ_i is the reactance slope at ω_i.
2) Nonresonating reactance—to account for NRNs in the coupling diagram—of different type:
   a) inductive NRN with inductance χ_i—when $\omega_{i1} = 1$ and $\omega_{i2} = 0$;
   b) capacitive NRN with capacitance χ_i^{-1}—when $\omega_{i1} \to \infty$ and $\omega_{i2} = 1$;
   c) frequency-invariant NRN—when $\omega_{i1} = \omega$ and $\omega_{i2} = 0$, being zero if $\chi_i = 0$ is also satisfied.

   Note that a combination of a capacitive or inductive and constant values in the NRNs is also admissible.

Nonresonating modes [35] can also be considered by this general synthesis framework, as they can be either treated as resonators with ω_i being away from the passband or approximated by NRNs. In relation to the formula (14), it should be pointed out that it can be replaced by a more complex frequency-dependent expression for the node reactance, such as the one associated with a set of resonators—e.g., doublet, triplet, or quadruplet. In this case, the node in the network may be regarded as a higher level node describing a whole building block that is possibly predesigned. Note that using building blocks or constituent sections is a popular approach for creating complex filtering networks, and this technique can easily be accommodated in the model and the INEVP framework proposed in this article.

The reactances, as well as the source and load, are all coupled by inverters that can be either constant or frequency-variant. At this stage, it is assumed that the inverters are ideal in the sense that the diagonal elements of their open-circuit impedance parameters are zero—the modifications to be considered for the frequency-dependent case are discussed later. With regard to the kind of frequency dependence of the off-diagonal elements, three different categories are defined depending on their frequency-derivative behavior as follows.

1) FII—when the first and higher-order derivatives vanish everywhere.
2) LFVI—when the first derivative is nonzero, and the second-order and higher order derivatives vanish everywhere.
3) AFVI—when the second derivative or any higher order derivative is nonzero.

To denote the different categories of nodes and inverters to be used in a coupling-routing diagram, the representation convention of symbols shown in Fig. 2 is adopted here.

The reactance matrix $\mathbf{X}(\omega)$ for the network shown in Fig. 1 has two extra rows and columns—so its dimension is

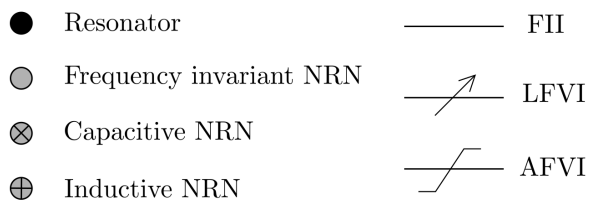

Fig. 2. Convention of symbols of nodes and inverters used in coupling-routing diagrams.

$(N+2)\times(N+2)$—as follows:

$$\mathbf{X}(\omega)=\begin{bmatrix} x_{SS} & x_{S1} & x_{S2} & \cdots & x_{SN} & x_{SL} \\ x_{S1} & x_{11} & x_{12} & \cdots & x_{1N} & x_{1L} \\ \vdots & \vdots & \vdots & \ddots & \vdots & \vdots \\ x_{SN} & x_{1N} & x_{2N} & \cdots & x_{NN} & x_{NL} \\ x_{SL} & x_{1L} & x_{2L} & \cdots & x_{NL} & x_{LL} \end{bmatrix}. \quad (15)$$

The diagonal entries in this matrix are given by $jx_{ii}=jX_i$. For practical reasons, it is convenient to normalize the coupling matrix as it is done in the conventional synthesis of the frequency-invariant coupling matrix in the prototype domain. To normalize rows and columns, the source R_S and load R_L resistances, the fractional bandwidth Δ, and the parameter χ (reactance slope for resonators and inductance or inverse of capacitance for inductive or capacitive NRNs, respectively) are used. The normalization process is carried out by left and right multiplying the coupling matrix by diagonal matrices $\mathbf{Q}$, where the diagonal entries of the $\mathbf{Q}$ matrix are given by

$$q_{SS}=R_S^{-1/2},\quad q_{LL}=R_L^{-1/2} \quad (16)$$

$$q_{ii}=\begin{cases}\chi_i^{-1/2}\Delta^{-1/2}, & \text{when } \chi_i\neq 0\\ 1, & \text{otherwise.}\end{cases} \quad (17)$$

After introducing this normalization, the following expression is obtained for the extended coupling matrix:

$$\mathbf{M}=\mathbf{Q}\mathbf{X}(\omega)\mathbf{Q}. \quad (18)$$

Besides, for the termination impedance matrix $\mathbf{R}$ in (13), it is also normalized. Observe that when all the inverters are frequency-invariant, all the coupled reactances are considered to be identical—i.e., synchronously tuned resonators with $\omega_{0i}=\omega_0$—, and no NRNs are present in the filter network; the coupling matrix adopts the well-known form that is commonly used in the traditional synthesis in the low-pass prototype domain. In addition, it is noteworthy to notice that the normalization process does not affect the localization of the roots of the characterization equation so that the diagonal elements of matrix $\mathbf{Q}$ can be chosen differently. For instance, the normalization for NRNs can be performed as in [36].

Note that the model introduced here is much more general than the one proposed in [6]—which only addressed couplings that are either constant or inversely proportional to frequency—or the one in [7]—where a combination of frequency-dependent couplings proportional or inversely proportional to frequency (either capacitive or inductive) was considered. Such constraints on the type of frequency dependence for couplings are overcome by the proposed synthesis method.

A. Loading Effect Due to Nonideal Inverters

The matrix derived above can be used in the inverse eigenvalue problem to find the parameters that are required to fulfill the filter specification. It is, however, convenient to consider the effect of the loading reactances on the main diagonal when the inverters are nonideal. By a nonideal inverter, it is understood a two-port reactive coupling network characterized by its open-circuit impedance parameters; nevertheless, unlike for ideal inverters, which do not have the Foster representation and are mathematical concepts that facilitate filter design, these coupling networks are reactive two-port circuits and have nonzero diagonal entries in their impedance-parameter description. For example, if the coupling between reactances i and k is considered, the reactive coupling network associated with it can be described by the following open-circuit impedance matrix:

$$\mathbf{Z}_{ik}=\begin{bmatrix} z_{ik}^{11} & z_{ik}^{12} \\ z_{ik}^{12} & z_{ik}^{22} \end{bmatrix}. \quad (19)$$

The diagonal elements will load both reactances, and this can be considered in the coupling-matrix definition. Note that each reactance can be coupled to other reactances so that all the nonideal inverters that load each reactance considered. Like for ideal inverters, frequency-invariant (i.e., constant) couplings (FICs) and the two categories of dispersive couplings—LFVCs and AFVCs—are distinguished. The open-circuit impedance matrix of the AFVC must have the Foster representation as in (1). As noted above, in order to compensate for the loading effect due to any of these couplings, the reactances will have to be modified. It is useful to reflect this effect in the coupling matrix so that the loading effect is expressed in an explicit way. To this end, the coupling matrix is decomposed into three parts as follows:

$$j\mathbf{X}(\omega)=j\mathbf{X}^x+j\mathbf{X}^l+j\mathbf{X}^I \quad (20)$$

where $\mathbf{X}^x$ is the diagonal matrix of reactances, $\mathbf{X}^l$ is the diagonal matrix that accounts for the cumulative loading effect due to all the nonideal inverters, and $\mathbf{X}^I$ is a matrix with zeros on the diagonal that describes the coupling provided by ideal inverters, in general with arbitrary frequency variation

$$\mathbf{X}^x=\text{diag}[X_S,X_1,X_2,\ldots,X_N,X_L] \quad (21)$$

$$\mathbf{X}^l=\text{diag}\left[x_{SS}^l,x_{11}^l,\ldots,x_{NN}^l,x_{LL}^l\right] \quad (22)$$

with

$$jx_{kk}^l=\sum_{l=k+1}^{N+2}z_{kl}^{11}+\sum_{l=0}^{k-1}z_{kl}^{22} \quad (23)$$

and

$$jx_{ik}^I=-z_{ik}^{12},\quad i\neq k \qquad jx_{kk}^I=0. \quad (24)$$

Note that in the above equations $i,k=0,1,\ldots N+1$ and, for the sake of compactness in (23) and (24), i, k, or $l=0$ is assigned to the source and i,k, or $l=N+1$ refers to the load.

The above expression defines the component of the nonnormalized coupling matrix. Practical computation involves

normalized component matrices and the entire normalized coupling matrix is

$$\mathbf{M} = \mathbf{Q}\mathbf{X}(\omega)\mathbf{Q} = \mathbf{M}^x + \mathbf{M}^l + \mathbf{M}^I. \tag{25}$$

As a final remark, note that the elements of the matrix $\mathbf{M}^l$ are not optimizable when the IEVP is solved. This is because their values are a function of variables related to the off-diagonal elements of the open-circuit impedance parameters of the inverters contained in the matrix $\mathbf{X}^I$. Consequently, entries in $\mathbf{M}^l$ change implicitly as a result of variations in $\mathbf{M}^I$.

B. Coupled-Resonator Filter Synthesis Step by Step

Given the filter specifications (bandwidth, center frequency, return-loss level, location of TZs, filter order n, number of nodes N and network topology, formulas for reactances and characteristics of the AFVC elements—passive two-port networks with open-circuit impedance matrix with frequency dependence according to the Foster representation in (1)—, and a chosen reference model as discussed in the previous section—e.g., short-circuit admittance parameters, scattering parameters, or eigenvalues of the reference frequency-invariant network), the following steps have to be executed assuming that the reference model is associated with the poles and zeros of y_{11} and y_{22} or $S_{11} - 1$ and $S_{22} - 1$.

Step 1. Based on the desired transmission characteristics and the filter order, synthesize three polynomials for the numerators and denominator of the reference filter-network model.

Step 2. Define three sets of reference roots as follows: $\boldsymbol{\omega}_p$ with the reference poles associated with eigenvalues of the entire target coupling matrix, $\boldsymbol{\omega}_u$ with the reference zeros associated with the eigenvalues of the upper principal submatrix of the target filter model, and $\boldsymbol{\omega}_l$ with the reference zeros associated with the eigenvalues of the lower principal submatrix.

Step 3. Evaluate the normalization coefficients for the rows and columns of the coupling matrix.

Step 4. Solve the INEVP by optimization. The goal function for the optimization is given by

$$C = \|\boldsymbol{\lambda}_u - \boldsymbol{\omega}_u\| + \|\boldsymbol{\lambda}_l - \boldsymbol{\omega}_l\| + \|\boldsymbol{\lambda} - \boldsymbol{\omega}_p\|$$

where $\boldsymbol{\lambda}$, $\boldsymbol{\lambda}_u$, and $\boldsymbol{\lambda}_l$ are vectors of eigenvalues of the coupling matrix and its two principal submatrices.

Step 5. Denormalize the elements of the coupling matrix to get the values of the reactance part of the network as

$$\mathbf{X} = \mathbf{Q}^{-1}\mathbf{M}(\omega)\mathbf{Q}^{-1}. \tag{26}$$

Some additional remarks to be considered are given as follows.

Remark 7: The choice of the reference sets is somehow arbitrary. They can be selected according to the needs, and they can also be the roots associated with bottom-left or top-right principal submatrices (e.g., for S_{21}) or even as central principal submatrix (poles of y_{11}, y_{21}, and y_{22} in the extended coupling matrix). Note also that for lossy or nonreciprocal [31] networks—which are not discussed in this work—, a total of four sets is needed.

Remark 8: Due to the presence of AFVCs or NRNs, the size of the coupling matrix to be synthesized, that is, $(N + 2) \times (N + 2)$, is not equal to $(n + 2) \times (n + 2)$, where n is the degree of the network. In fact, as it will be seen in the synthesis examples provided in Section V, both $n > N$ and $n < N$, as well as $n = N$, are possible.

Remark 9: The INEVP is solved in the passband domain, but the synthesis of the polynomials can be carried out in the low-pass filter domain and, then, the reference sets can be transformed to the passband domain. This is recommended as the polynomial synthesis in the low-pass domain is more stable numerically than in the passband domain.

Remark 10: The reference polynomials have to be known; for instance, these polynomials can be synthesized analytically or by optimization. Examples include polynomials for filtering functions involving arbitrary locations of TZs [6], [7], polynomials for dispersive delay structures (DDSs) with controlled magnitude [37], or even functions with $n + 1$ TZs that can be achieved by adding a resonant-type source–load coupling [14].

Remark 11: During the optimization process needed to obtain the INEVP solution, splitting (25) may be used so that each design parameter can be altered independently. The optimizable parameters can be related to reactances at the filter nodes (e.g., resonant frequency ω_{0i}) and to the coupling networks (parameters controlling the off-diagonal elements of the frequency-variant couplings $\mathbf{M}^I$). As noted before, the diagonal elements of the couplings, which are collected in the matrix $\mathbf{M}^l$, are in general not optimizable, and they change whenever the elements of $\mathbf{M}^I$ are altered in order to ensure that the coupling network preserves a reactive-type character. It is also possible to assign the parameter χ_i in some or all nodes as an optimization variable. In this case, the element of the normalization matrix $\mathbf{Q}$ in (17) corresponding to this node needs to be replaced by an arbitrary scaling constant $(\chi_i^0)^{1/2}$.

Remark 12: The synthesis procedure will not converge in the following situations.

1) The desired specification cannot be achieved with the assumed coupling scheme and type of frequency-variation profile for the open-circuit impedance parameters of the coupling networks.
2) The number of eigenvalues of the coupling matrix or its principal submatrices is different from the number of reference zeros and poles.

IV. Arbitrary Frequency-Variant Couplings

As previously mentioned, the proposed synthesis framework is fully general for the design of microwave filters with coupling networks exhibiting arbitrary frequency-variant profiles. Nevertheless, for illustration purposes of the engineered filter synthesis methodology, three particular cases of frequency-variant coupling topologies are considered here.

The circuit configurations of the three selected examples of AFVC networks are shown in Fig. 3. As can be seen, they consist of reciprocal two-port circuits—which are also symmetrical for the cases shown in Fig. 3(a) and (b)—, whose electrical behavior can be represented by means of their impedance-parameter matrix as follows.

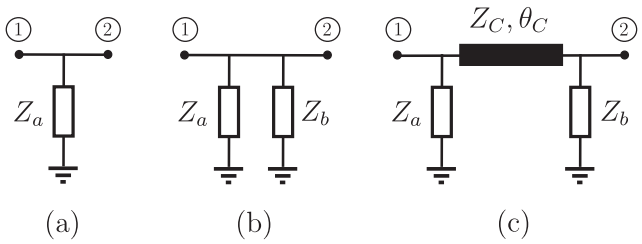

Fig. 3. Examples of two-port circuits corresponding to AFVC networks (the impedances Z_a and Z_b and the electrical length θ_C of the transmission-line segment are assumed to be frequency-dependent). (a) Type I: shunt impedance. (b) Type II: two in-parallel shunt impedances. (c) Type III: two shunt impedances separated by a transmission-line segment.

1) *Type I:* Shunt impedance $Z_a = Z_a(\omega)$—i.e., Fig. 3(a)

$$Z_{11}(\omega) = Z_{22}(\omega) = Z_{21}(\omega) = Z_a. \tag{27}$$

2) *Type II:* Two shunt impedances $Z_a = Z_a(\omega)$ and $Z_b = Z_b(\omega)$ that are connected in parallel—i.e., Fig. 3(b)

$$Z_{11}(\omega) = Z_{22}(\omega) = Z_{21}(\omega) = \frac{Z_a Z_b}{Z_a + Z_b}. \tag{28}$$

3) *Type III:* Two shunt impedances $Z_a(\omega)$ and $Z_b(\omega)$ that are separated by a transmission-line segment with characteristic impedance $Z_C = 1/Y_C$ and frequency-dependent electrical length $\theta_C = \beta(\omega)l$ (where $\beta(\omega)$ and l are the phase constant and the physical length of the transmission-line segment, respectively)—i.e., Fig. 3(c)

$$\begin{aligned} Z_{11}(\omega) &= \frac{Z_a Z_b + j Z_a Z_C \tan\theta_C}{(Z_a + Z_b) + j(Z_C + Y_C Z_a Z_b)\tan\theta_C} \\ Z_{22}(\omega) &= \frac{Z_a Z_b + j Z_b Z_C \tan\theta_C}{(Z_a + Z_b\ ) + j(Z_C + Y_C\ Z_a\ Z_b)\tan\theta_C} \\ Z_{21}(\omega) &= \frac{Z_a Z_b/\cos\theta_C}{(Z_a + Z_b) + j(Z_C + Y_C Z_a Z_b)\tan\theta_C}. \end{aligned} \tag{29}$$

Note that if $\theta_C = 0$, then the Type-III coupling network becomes the Type-II one.

It should be remarked upon that these three types of frequency-variant coupling networks can exhibit different behavior in terms of transmission zero and pole generation. For example, if the impedances Z_a and Z_b are realized by means of open-ended transmission-line segments or stubs so that

$$Z_a(\omega) = -jZ_A/\tan(\omega\theta_{A0}/\omega_0) \tag{30}$$

$$Z_b(\omega) = -jZ_B/\tan(\omega\theta_{B0}/\omega_0) \tag{31}$$

where Z_A and Z_B are the characteristic impedances and θ_{A0} and θ_{B0} are the electrical lengths at ω_0 of the transmission-line segments, and then, the following features are obtained for the coupling networks in Fig. 3 that can be adjusted independently.

1) *Type I:* One TZ at $\omega_z = \omega_0\pi/(2\theta_{A0})$.
2) *Type II:* Two TZs at $\omega_{z1} = \omega_0\pi/(2\theta_{A0})$ and $\omega_{z2} = \omega_0\pi/(2\theta_{B0})$ with one pole between them at ω_p so that $Z_a(\omega_p) = -Z_b(\omega_p)$.
3) *Type III:* Two TZs at $\omega_{z1} = \omega_0\pi/(2\theta_{A0})$ and $\omega_{z2} = \omega_0\pi/(2\theta_{B0})$, being both below or above one pole at ω_p—or even each of them at one different side with regard to the pole location as for the case $\theta_C = 0$.

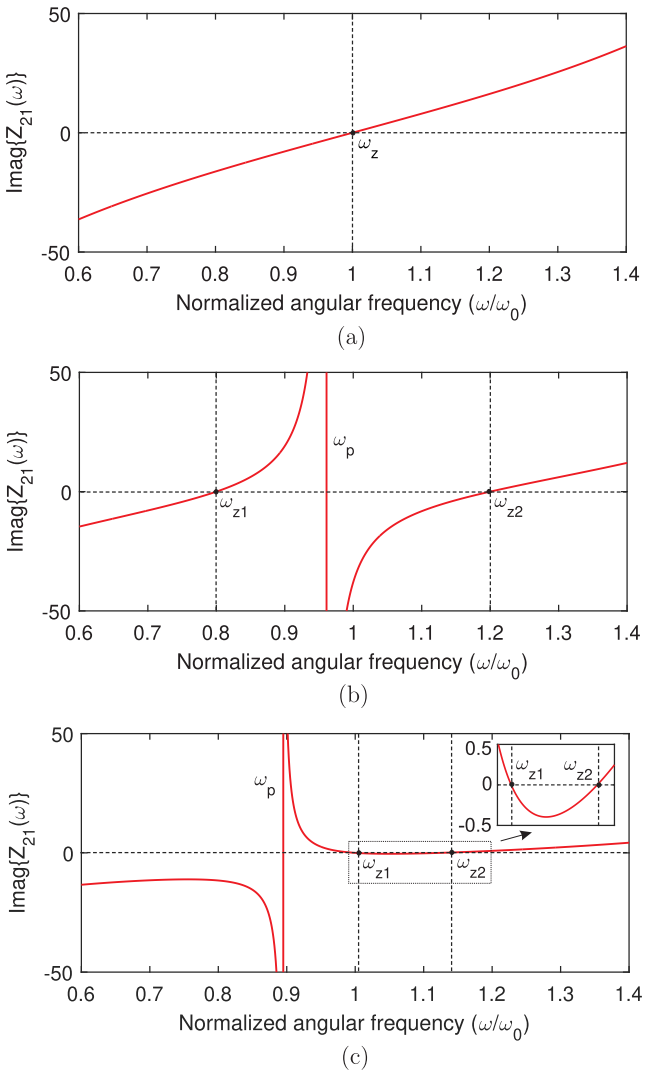

Fig. 4. Examples of Z_{21} parameter—imaginary part—for the frequency-variant coupling networks in Fig. 3 ($Z_0 = 50\ \Omega$). (a) Type-I coupling network in Fig. 3(a) ($Z_A = Z_0$ and $\theta_{0A} = \pi/2$). (b) Type-II coupling network in Fig. 3(b) ($Z_A = Z_0$, $\theta_{0A} = 0.625\pi$, $Z_B = Z_0$, and $\theta_{0B} = 0.4167\pi$). (c) Type-III coupling network in Fig. 3(c)—both TZs are produced above the pole: $Z_A = 0.78Z_0$, $\theta_{0A} = \pi/2$, $Z_B = 0.4Z_0$, $\theta_{0B} = 0.4444\pi$, $Z_C = 1.3Z_0$, and $\theta_{0C} = 0.0722\pi$.

For illustration purposes, Fig. 4 shows the examples of the transimpedance parameter Z_{21} (imaginary part) for the three types of frequency-variant coupling networks in Fig. 3, where the aforementioned properties in terms of TZ and pole generation are verified. Note also that, due to the inherent frequency-periodic behavior of the transmission-line segments building these coupling networks, additional TZs and poles are created at other frequency ranges, despite that their spectral positions cannot be controlled independently.

V. Synthesis Examples

This section presents the synthesis results of seven different bandpass filter architectures using a variety of frequency-dependent couplings or NRNs. The provided examples include six inline topologies and one quadruplet. In all these examples, the reference poles and zeros were determined from the targeted filtering functions, which were constructed

TABLE I

RESONANT FREQUENCIES FOR NODES $f_i = (\omega_i/2\pi)$ (IN GHz), STUB IMPEDANCES (IN Ω), AND THEIR ELECTRICAL LENGTHS AT f_0 (IN DEGREES) (THIRD-ORDER BANDPASS FILTERS WITH TWO TZs)

Topology in Fig. 5	f_1	f_2	f_3	f_4	f_5	Z_{s1}	Z_{s2}	θ_1	θ_2	Z_C	θ_C
(a) LFVC	2.446	2.395	2.328	-	-	153.096	92.454	95.575	82.442	-	-
(b) Type-I AFVC	2.446	2.395	2.329	-	-	158.716	89.394	95.602	82.552	-	-
(c) NRN	2.387	-	2.620	2.260	2.387	-	-	-	-	-	-
(d) Type-II AFVC	2.387	2.387	-	-	-	80.330	48.337	95.600	82.540	-	-
(d) Type-III AFVC	2.372	2.400	-	-	-	27.569	13.894	82.446	76.596	83.705	4.012

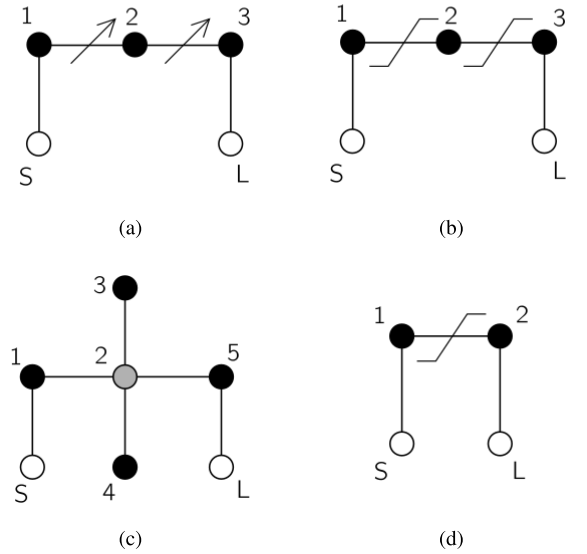

Fig. 5. Coupling-routing diagrams for the third-order bandpass filter examples. (a) Three resonators with two LFVCs. (b) Three resonators with two AFVCs. (c) Four resonators with one NRN. (d) Two resonators with one AFVC.

using the analytical procedure described in [5]. The coupling matrix was split as indicated in (25). In all those examples that involve dispersive couplings (either LFVC or AFVC of Type-I, Type-II, and Type-III), nonzero diagonal elements in their open-circuit impedance-parameter matrices were introduced as previously discussed. Consequently, when solving the associated INEVP, the resonant frequencies ω_i in (14) in the matrix $\mathbf{M}^x$ were exploited as optimizable parameters to compensate for the loading effect of the imperfect inverters (matrix $\mathbf{M}^I$). The elements of the matrix $\mathbf{M}^I$ were also considered optimizable variables, while the entries of the matrix $\mathbf{M}^l$ changed only implicitly as a result of modifications in $\mathbf{M}^I$.

A. Third-Order Filters With Two Transmission Zeros

To illustrate the capabilities of the proposed synthesis method based on INEVP for various types of dispersive couplings and topologies involving NRNs, five distinct examples of synthesized third-order bandpass filters with two TZs are provided here. In each case, it is assumed that the center frequency and bandwidth are 2.4 and 0.15 GHz (i.e., 6.25% in relative terms), respectively, while the minimum in-band return-loss level is 20 dB. For the first-to-four filters, the TZs are placed at 2.26 and 2.62 GHz (i.e., at both sides of the passband). Specifically, the four configurations considered for these four bandpass filter examples are as follows.

1) Three resonators with two LFVCs: Fig. 5(a).

TABLE II

VALUES OF FREQUENCY-INVARIANT COUPLINGS (THIRD-ORDER BANDPASS FILTERS WITH TWO TZs)

Topology in Fig. 5	m_{S1}	m_{NL}	m_{12}	m_{23}	m_{24}	m_{25}
(a) LFVC	1.415	1.327	-	-	-	-
(b) Type-I AFVC	1.416	1.327	-	-	-	-
(c) NRN	1.178	1.178	0.809	1.197	0.891	0.809
(d) Type-II AFVC	1.178	1.178	-	-	-	-
(d) Type-III AFVC	1.147	1.142	-	-	-	-

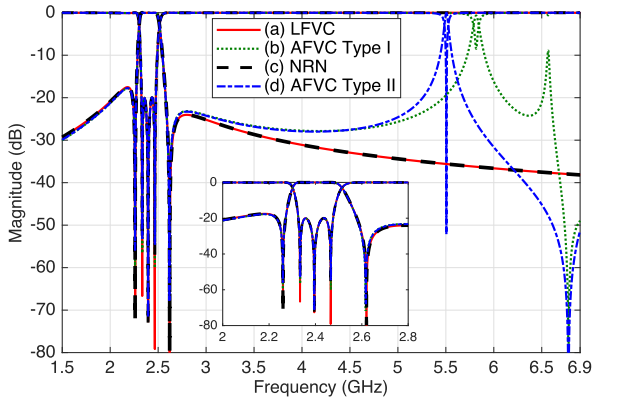

Fig. 6. Power transmission ($|S_{21}|$) and reflection ($|S_{11}|$) responses of the third-order bandpass filter examples with two TZs (one TZ at each passband side) computed from the synthesized coupling matrix for four different implementations involving FVCs or NRNs: Fig. 5(a)–(d)—the inset shows the responses near the passband range. (Note that curves (a) and (c) are overlapping.)

2) Three resonators with two Type-I AFVCs: Fig. 5(b).
3) Four resonators with one NRN: Fig. 5(c).
4) Two resonators with one Type-II AFVC: Fig. 5(d).

In the fifth bandpass filter example, the two TZ are positioned above the passband at 2.62 and 2.82 GHz, for which two resonators that produce two poles and one Type-III AFVC that generates the two TZs and one pole are employed. The coupling-routing topology for this filter is shown in Fig. 5(d). Hence, all three types of coupling networks shown in Fig. 3 are considered in these filter examples.

As can be inferred from the description above, even though the specification for the bandpass filter example with two TZs at both sides of the passband is the same, the way in which the TZs are obtained in each design is different. In particular, the dispersive couplings exhibit different frequency-variation patterns. For reference, the first filter example is synthesized in the low-pass prototype domain by using the assumption of linear frequency dependence for the inverters, and the procedure described in [13] and [15] is used. It involves the solution of the generalized IEVP in (3). In all other cases, the synthesis is performed in the bandpass domain and the new INEVP framework outlined above is employed. The final design parameter values resulting from the synthesis for all

these third-order bandpass filter examples are given in Tables I and II, while their power transmission and reflection responses derived from the synthesis process are compared in Fig. 6. In this figure, the representation of these responses in a broad frequency interval is given, whereas the inset shows their detail in the vicinity of the passband. As demonstrated, between 2 and 2.8 GHz, the coupling-matrix responses of the four examples exactly match the filter specifications (characterization obtained directly from the rational representation of the prototype response). The differences among them are clearly visible above 3 GHz, where the characteristics for the designs involving AFVCs deviate from the desired one. This is a natural consequence of the nonlinear and periodic frequency-variation patterns of the inverter parameters. It has to be pointed out that the results given in Table I clearly show that the resonators are detuned, as a result of the loading effect due to the nonideal inverters.

Note that the results given in Tables I and II show that the designs involving three resonators and two FVCs [see Fig. 5(a) and (b)] differ, even though the dispersive couplings are implemented as shunt open-ended stubs in both examples—each stub is quarter-wavelength long at the TZ frequency generated by it and shows a nonlinear frequency-variation profile in its equivalent impedance. For the sake of illustration, in the coupling scheme in Fig. 5(a), such impedance was approximated by a linear function of frequency—which is a relatively accurate approximation for this type of stub—, where its slope is determined by the characteristic impedance. In the second design [see Fig. 5(b)], the stub impedance was not approximated by a linear function of frequency. Thus, the stubs were modeled as AFVCs with the Type-I coupling network. Accordingly, the synthesis was carried out in this case by considering an INEVP. After reaching convergence, the values for the stub impedances were found to be 158.72 and 89.40 Ω. This result is slightly different from what was obtained by linearization (153.10 and 92.45 Ω), and this is due to the different models of the frequency-variant inverters.

The implementations involving four resonators and one NRN [see Fig. 5(c)] and two resonators with one Type-II AFVC [see Fig. 5(d)] lead to designs with identical m_{S1} and m_{NL}. In fact, the middle section in the design with one NRN produces one pole and two TZs [38]. They are created at exactly the same locations as for the Type-II AFVC. However, while the locations of the TZs in the NRN section are the same as the resonant frequencies of resonators 3 and 4, they are determined by the lengths of the stubs in the AFVC.

Concluding the discussion related to the synthesis of the bandpass filter examples with two TZs at both sides of the passband, two major points must be highlighted. First, the convergence of INEVP process solution in all these cases was found to be very quick. This is shown in Fig. 7. It has to be noted, however, that the number of iterations depends on the starting point. For the results presented in Fig. 7, the initial values were quite far from the final ones (which is evident from the high value of the goal function at the first iteration, as shown in the plot). The second aspect is the number of eigenvalues (M) versus the number of nodes

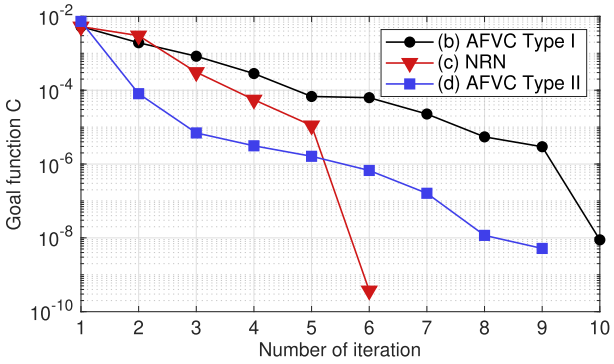

Fig. 7. Convergence of the optimization procedure for solving the INEVP—third-order bandpass filter examples with two TZs at both sides of the passband.

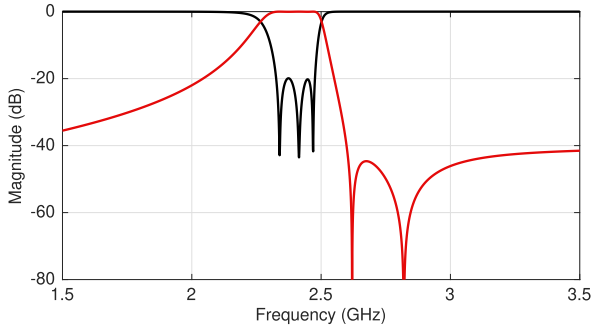

Fig. 8. Power transmission ($|S_{21}|$) and reflection ($|S_{11}|$) responses of the third-order bandpass filter example with two TZs above the passband using one Type-III AFVC: Fig. 5(d).

(N) in the network and the filter order n ($n = 3$ in all the examples considered above). For the first structure with two LFVCs, the number of finite eigenvalues of the coupling matrix matches the number of nodes (three in this case) so that $M = N = n$. In the implementation involving Type-I AFVCs, $M = N = n$ is also satisfied; however, the number of eigenvalues of the INEVP depends on the frequency range—it is three when the interval is not too wide (e.g., 1.5–3 GHz) and increases to five when the frequency range is extended up to 7 GHz. For the structure with the NRN, $N = 5$ and $M = 5$, while $n = 3$ (i.e., $M = N > n$); here, the two extra eigenvalues are at infinity and the number of eigenvalues is the same regardless of the considered frequency range. In the implementation involving two resonators and one Type-II AFVC, there are two nodes in the network, while the filter order is three, so that $n > N$. In such case, the INEVP gives three eigenvalues when considering the frequency range 1.5–3 GHz ($M = n > N$) and four when the upper limit is set to 7 GHz, thus resulting in $M > n > N$.

The last example of third-order bandpass filter is an inline filter with one Type-III AFVC [see Fig. 5(d)]. In this case, both TZs were imposed to be placed above the passband, as it can be seen in the filter transfer function drawn in Fig. 8. The optimization procedure converged in 17 steps for this example. The final result of the optimization is shown in Tables I and II.

B. Higher Order Filters With AFVCs and NRNs

As more challenging examples, the synthesis of higher order bandpass filters with multiple TZs is subsequently addressed.

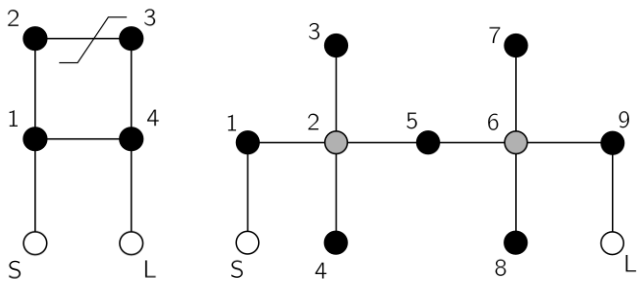

(a) (b)

Fig. 9. Coupling-routing diagrams for the fifth-order bandpass filter examples. (a) Four resonators with one AFVC. (b) Seven resonators with two NRNs.

The first example consists of a fifth-order bandpass filter with four resonators and one Type-II AFVC. Similar to the previous example of the third-order bandpass filter with one Type-II AFVC, the number of nodes is smaller than the order of the filter (i.e., $N < n$). The center frequency is 3 GHz, the absolute bandwidth is 120 MHz (i.e., fractional bandwidth equal to 4%), the minimum in-band return-loss level is 20 dB, and its three TZs are imposed to be positioned at 2.85, 3.12, and 3.25 GHz. Its coupling-routing diagram is shown in Fig. 9(a), which corresponds to a quadruplet with one cross-coupling between resonators 1 and 4. In this network, two symmetrically located TZs are inherently produced by the quadruplet with FIIs. In addition, by replacing the coupling between resonators 2 and 3 with the Type-II AFVC, the filter order is increased by one and one additional TZ is created above the passband. Note also that there is no symmetry in the location of TZs. In this case, the solution of the INEVP was obtained after 21 iterations, leading to the following final solution: $f_1 = f_4 = 2.999$ GHz, $f_2 = f_3 = 3.008$ GHz, $Z_{s1} = 10.861\ \Omega$, $Z_{s2} = 31.631\ \Omega$, $\theta_1 = 96.819^{\circ}$, $\theta_2 = 87.013^{\circ}$, $m_{S1} = m_{4L} = 1.001$, $m_{12} = m_{34} = 0.889$, and $m_{14} = 0.018$. The response of the filter is shown in Fig. 10(a).

The second example is another fifth-order bandpass filter, but in this case, its associated coupling network comprises a total of seven resonators and two NRNs. The coupling-routing diagram of the filter is shown in Fig. 9(b). Each set shaped by an NRN and its two adjoining resonators produces one pole and two TZs. The filter is centered at 3.5 GHz, its bandwidth is equal to 300 MHz (i.e., 8.57% in relative terms), its minimum in-band return-loss level is equal to 20 dB, and the positions of its four TZs are set at 3.1, 3.2, 3.75, and 4 GHz. The final result of the optimization is as follows: $f_1 = 3.495$ GHz, $f_3 = 101$ GHz, $f_4 = 4.000$ GHz, $f_5 = 3.506$ GHz, $f_7 = 3.200$ GHz, $f_8 = 3.750$ GHz, $f_9 = 3.526$ GHz, $m_{S1} = 1.051$, $m_{12} = 0.470$, $m_{23} = 1.024$, $m_{24} = 1.088$, $m_{25} = 0.355$, $m_{56} = 0.533$, $m_{67} = 0.984$, $m_{68} = 0.783$, $m_{69} = 0.781$, and $m_{9L} = 1.159$. Fig. 10(b) shows the response of the filter. In this case, the solution of the INEVP required 27 iterations.

VI. Experimental Results

For practical validation purposes, one of the filter synthesis examples presented in Section V has been manufactured in microstrip technology and characterized. It corresponds to a

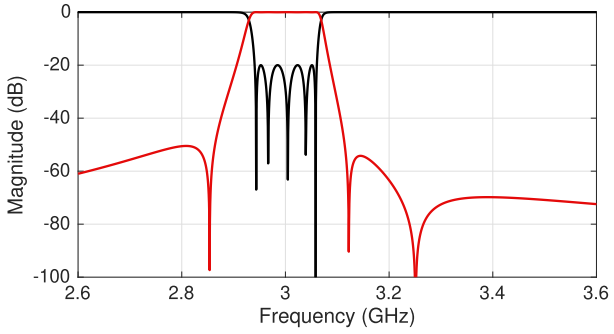

(a)

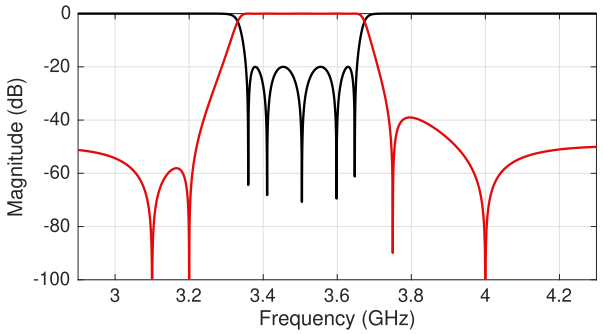

(b)

Fig. 10. Power transmission ($|S_{21}|$) and reflection ($|S_{11}|$) responses of the fifth-order bandpass filter examples. (a) Quadruplet with one Type-II AFVC. (b) Seven resonators with two NRNs.

third-order bandpass filter design shaped by two resonators and one inter-resonator Type-II AFVC, which adds the two finite TZs and increases the filter order by one. The prefixed specifications are those that were previously indicated.

By using the coupling-matrix parameters given in Tables I and II, the filter was implemented as a distributed-element circuit network shaped by the following elements: two quarter-wavelength open-ended transmission lines corresponding to two series-type resonators (the additional 0.5°-long line segments are added to make them to exactly resonate at 2.387 GHz in accordance with the theoretical synthesis results), two open-ended stubs associated with the Type-II AFVC, and input and output couplings realized through parallel-coupled-line stages. The ideal transmission-line circuit schematic of the filter is shown in Fig. 11. Its theoretical power transmission and reflection parameters, along with those corresponding to its associated coupling-matrix synthesis, are plotted in Fig. 12.

The layout—with indication of dimensions—and a photograph of the developed microstrip filter prototype are shown in Fig. 13. For circuit manufacturing, an Isola 680-338 substrate with the following parameters was used: relative dielectric permittivity $\varepsilon_r = 3.38$, dielectric thickness $H = 0.762$ mm, metal thickness $t = 17.5\ \mu$m, and dielectric loss tangent $\tan(\delta_D) = 0.0035$. Although the obtained theoretical values for the different filter parameters were exploited as the initial solution for the dimensional synthesis, their dimensions were finely adjusted with the zero–pole optimization technique available in the 3-D finite-element-method electromagnetic software package InventSim. The final

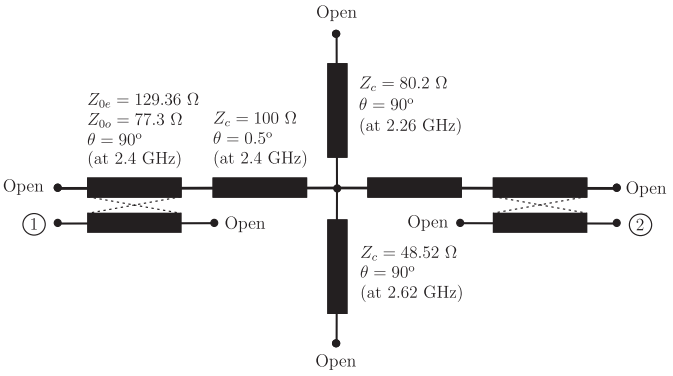

Fig. 11. Circuit schematic of the ideal transmission-line circuit realization of the third-order bandpass filter with one Type-II AFVC—topology in Fig. 5(d).

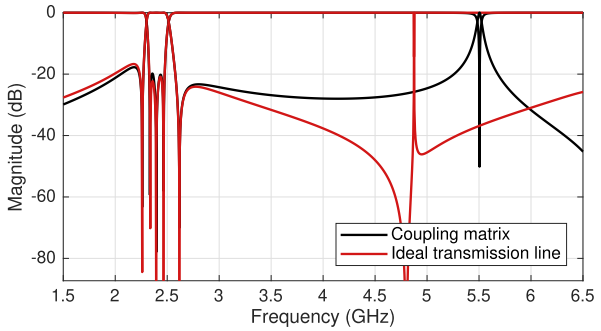

Fig. 12. Theoretical power transmission ($|S_{21}|$) and reflection ($|S_{11}|$) responses in a wide frequency interval of the transmission-line-based third-order bandpass filter with one Type-II AFVC along with those corresponding to its coupling-matrix synthesis—topology in Fig. 5(d).

simulations, considering the dielectric and conductor loss as well as the finite metal thickness, were carried out in ADS Momentum. The measurements were performed with a PNA-X N5242A network analyzer from Agilent Technologies.

The simulated and measured power transmission and reflection parameters of the manufactured microstrip filter prototype are compared in Fig. 14. As can be seen, apart from some discrepancies in terms of spectral shifting to a lower frequency range and some bandwidth reduction that are attributed to the tolerances of the manufacturing process and the relative dielectric permittivity, the filter principle is fairly verified. The main measured characteristics of the built filter prototype are as follows: center frequency of 2.377 GHz, 3-dB absolute bandwidth equal to 130 MHz—i.e., equal to 5.42% in relative terms—, minimum in-band power-insertion-loss level of 1.18 dB, minimum in-band power-matching level of 23.7 dB, and TZs located at 2.238 and 2.584 GHz.

VII. Discussion

The model and the synthesis technique proposed in this study have some restrictions. First of all, the reference zeros and polynomials have to be known. Currently, we find then using a classical low-pass prototype polynomial synthesis procedure, but it may not be sufficient for the same filters. Furthermore, even if the NEVP framework yields the zeros and poles associated with the spurious response, it cannot be directly considered in the synthesis process. The model is general, but the synthesis focuses on the region around the passband—i.e., the characteristics provided by the filtering

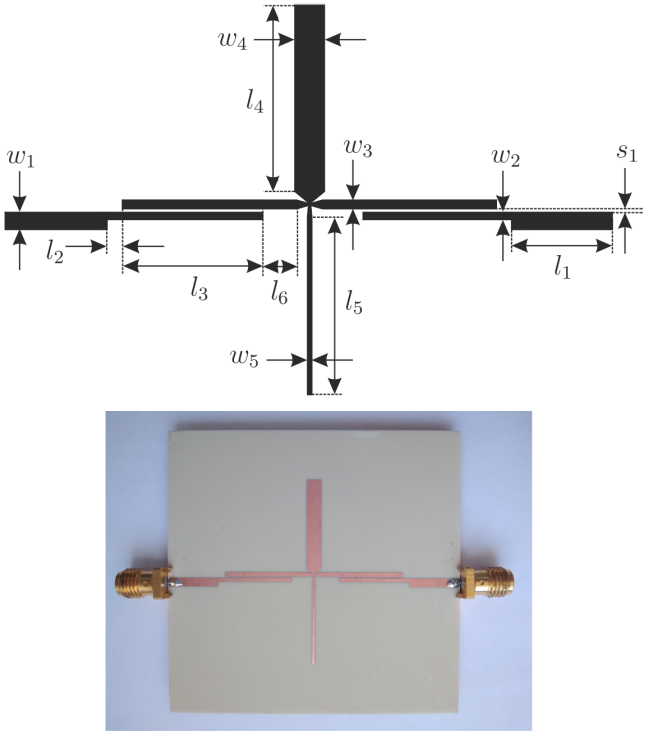

Fig. 13. Layout and photograph of the manufactured microstrip filter prototype (nonredundant dimensions in mm: $w_1 = 1.76$, $w_2 = 0.78$, $w_3 = 0.93$, $w_4 = 2.98$, $w_5 = 0.51$, $l_1 = 10$, $l_2 = 1.42$, $l_3 = 13.85$, $l_4 = 18.38$, $l_5 = 17.43$, $l_6 = 3.37$, and $s_1 = 0.27$; the taper connections in the cross junction are 1 mm long and terminate in 0.3 mm width).

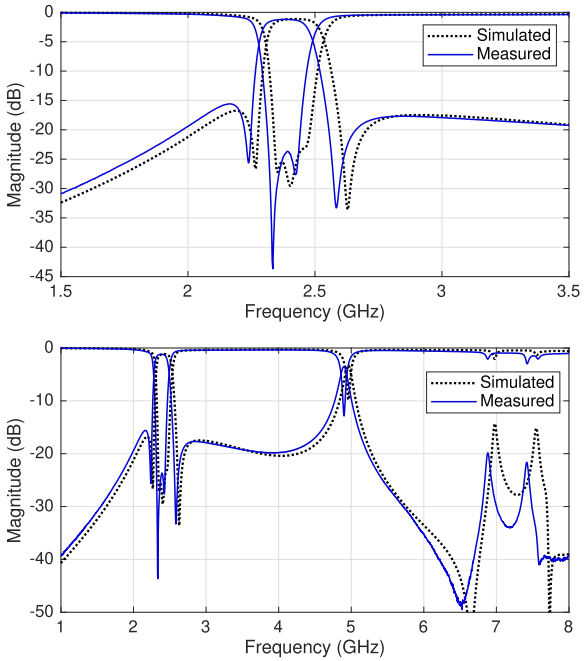

Fig. 14. Measured and simulated power transmission ($|S_{21}|$) and reflection ($|S_{11}|$) responses of the manufactured microstrip prototype corresponding to the third-order bandpass filter with one Type-II AFVC—topology in Fig. 5(d).

function. The locations of the spurious resonances are not known beforehand. Sometimes, such spurious resonances or bands can be estimated by examining the frequency characteristics of the constituent distributed elements, and certainly, they can be identified from the NEVP when the considered frequency range is wide enough. The spurious response can

be considered later on via optimization. Once the filter is synthesized according to the filtering function, the filter specification in the passband could be then kept as a constraint and the optimization may try to push away the spurious resonances/bands if needed by the intended application—this may be, however, indefeasible in the circuit representation that will always be an approximation of a full-wave electromagnetic response. Besides, an additional term can be added to the goal function in an attempt to push the spurious bands away.

Even if the model is more general than a traditional one, it can be regarded as a more restrictive model for a designer since the frequency characteristics of the coupling elements have to be decided upon very early on. This differs from the conventional approach, where the coupling matrix provides just the strength and sign of the coupling and a designer can later decide how to implement a particular coupling element.

Another drawback of the synthesis based on optimization is that, in general, any optimization method may fail to converge if a minimum cannot be reached from the assumed starting point. As the frequency profiles of the coupling elements can be arbitrary—as long as they are reactive networks—, general guidelines for the selection of a starting point cannot be formulated. However, engineering common sense seems to have worked for all the examples that have been synthesized to date using the technique based on the INEVP framework. It seems that the goal function based on zeros and poles is particularly well suited for optimization tasks related to filters, and it converges satisfactorily, as shown in Fig. 7. For full-wave-based design-by-optimization, the zero–pole goal function was exhaustively tested for random specifications and random starting points, showing excellent robustness for 300 trials as demonstrated in [39]. Still, even though the specifications and the starting points were random, engineering common sense was used to restrict the selectable ranges for these random picks. Finally, it must be remarked upon that the convergence will not be achieved if the minimum is not reachable for a given network topology and admissible frequency profiles for the coupling elements.

VIII. Conclusion

A new model for multicoupled-resonator filters with networks comprising nonideal AFVCs and NRNs was proposed. The synthesis procedure for determining the coupling matrix described by this general model was developed by using an inverse nonlinear eigenvalue framework. The synthesis process solves the associated INEVP by optimization and requires knowledge of the reference polynomials, whose roots can be matched to the characteristic frequencies of the filter parameters (i.e., zeros and poles). Its convergence requires that the solution is reachable for a preselected filter configuration and frequency-variation profiles of its coupling elements. The proposed model and synthesis technique are fully general, allowing for AFVCs, loaded or unloaded NRNs, nonresonating modes, frequency-dependent source–load coupling, multiple frequency-variant cross couplings, or even multiple dispersive couplings to connect the source/load to the filter network. Further research work to be carried out is the extension of this approach to more challenging filter topologies, such as multiband filters, multiport filtering devices (e.g., multiplexers or frequency channelizers), and filters with resistive elements (e.g., enhanced-in-band-amplitude-flatness lossy filters and reflectionless/absorptive filters).

References

[1] A. Atia, A. Williams, and R. Newcomb, "Narrow-band multiple-coupled cavity synthesis," *IEEE Trans. Circuits Syst.*, vol. CAS-21, no. 5, pp. 649–655, Sep. 1974.

[2] A. E. Atia and A. E. Williams, "Narrow-bandpass waveguide filters," *IEEE Trans. Microw. Theory Techn.*, vol. MTT-20, no. 4, pp. 258–265, Apr. 1972.

[3] R. J. Cameron, "General coupling matrix synthesis methods for Chebyshev filtering functions," *IEEE Trans. Microw. Theory Techn.*, vol. 47, no. 4, pp. 433–442, Apr. 1999.

[4] R. J. Cameron, "Advanced coupling matrix synthesis techniques for microwave filters," *IEEE Trans. Microw. Theory Techn.*, vol. 51, no. 1, pp. 1–10, Jul. 2003.

[5] R. Cameron, C. Kudsia, and R. Mansour, *Microwave Filters for Communication Systems*. New York, NY, USA: Wiley, 2007.

[6] S. Amari, F. Seyfert, and M. Bekheit, "Theory of coupled resonator microwave bandpass filters of arbitrary bandwidth," *IEEE Trans. Microw. Theory Techn.*, vol. 58, no. 8, pp. 2188–2203, Aug. 2010.

[7] W. Meng, H.-M. Lee, K. A. Zaki, and A. E. Atia, "Synthesis of wideband multicoupled resonators filters," *IEEE Trans. Microw. Theory Techn.*, vol. 59, no. 3, pp. 593–603, Mar. 2011.

[8] S. Amari, M. Bekheit, and F. Seyfert, "Notes on bandpass filters whose inter-resonator coupling coefficients are linear functions of frequency," in *IEEE MTT-S Int. Microw. Symp. Dig.*, Jun. 2008, pp. 1207–1210.

[9] U. Rosenberg, S. Amari, and F. Seyfert, "Pseudo-elliptic direct-coupled resonator filters based on transmission-zero-generating irises," in *Proc. Eur. Microw. Conf.*, 2010, pp. 962–965.

[10] S. Amari and J. Bornemann, "Using frequency-dependent coupling to generate finite attenuation poles in direct-coupled resonator bandpass filters," *IEEE Microw. Wireless Compon. Lett.*, vol. 9, no. 10, pp. 404–406, Oct. 1999.

[11] P. Kozakowski, A. Lamecki, M. Mongiardo, M. Mrozowski, and C. Tomassoni, "Computer-aided design of in-line resonator filters with multiple elliptical apertures," in *IEEE MTT-S Int. Microw. Symp. Dig.*, Jun. 2004, pp. 611–614.

[12] R. Levy, "New cascaded trisections with resonant cross-couplings (CTR sections) applied to the design of optimal filters," in *IEEE MTT-S Int. Microw. Symp. Dig.*, Jun. 2004, pp. 447–450.

[13] L. Szydlowski, A. Lamecki, and M. Mrozowski, "Coupled-resonator filters with frequency-dependent couplings: Coupling matrix synthesis," *IEEE Microw. Wireless Compon. Lett.*, vol. 22, no. 6, pp. 312–314, Jun. 2012.

[14] L. Szydlowski, A. Lamecki, and M. Mrozowski, "A novel coupling matrix synthesis technique for generalized Chebyshev filters with resonant source–load connection," *IEEE Trans. Microw. Theory Techn.*, vol. 61, no. 10, pp. 3568–3577, Oct. 2013.

[15] L. Szydlowski, N. Leszczynska, and M. Mrozowski, "Generalized Chebyshev bandpass filters with frequency-dependent couplings based on stubs," *IEEE Trans. Microw. Theory Techn.*, vol. 61, no. 10, pp. 3601–3612, Oct. 2013.

[16] Y. He *et al.*, "A direct matrix synthesis for in-line filters with transmission zeros generated by frequency-variant couplings," *IEEE Trans. Microw. Theory Techn.*, vol. 66, no. 4, pp. 1780–1789, Apr. 2018.

[17] Y. Zhang, F. Seyfert, S. Amari, M. Olivi, and K.-L. Wu, "General synthesis method for dispersively coupled resonator filters with cascaded topologies," *IEEE Trans. Microw. Theory Techn.*, vol. 69, no. 2, pp. 1378–1393, Feb. 2021.

[18] V. Zemlyakov, M. Tyaglov, and V. Shevchenko, "Compact quasi-elliptic waveguide filters on contoured resonant diaphragms," *J. Electromagn. Waves Appl.*, vol. 34, no. 2, pp. 224–234, Jan. 2020.

[19] M. Latif, G. Macchiarella, and F. Mukhtar, "A novel coupling structure for inline realization of cross-coupled rectangular waveguide filters," *IEEE Access*, vol. 8, pp. 107527–107538, 2020.

[20] H. Shaman and J.-S. Hong, "A novel ultra-wideband (UWB) bandpass filter (BPF) with pairs of transmission zeroes," *IEEE Microw. Wireless Compon. Lett.*, vol. 17, no. 2, pp. 121–123, Feb. 2007.

[21] M. Sánchez-Renedo, R. Gómez-García, and R. Loeches-Sánchez, "Microstrip filters with selectivity improvement using the new concept of signal-interference source/load coupling," in *IEEE MTT-S Int. Microw. Symp. Dig.*, Jun. 2013, pp. 1–4.
[22] X.-L. Huang, L. Zhou, M. Völkel, A. Hagelauer, J.-F. Mao, and R. Weigel, "Design of a novel quarter-mode substrate-integrated waveguide filter with multiple transmission zeros and higher mode suppressions," *IEEE Trans. Microw. Theory Techn.*, vol. 66, no. 12, pp. 5573–5584, Dec. 2018.
[23] D. Miek, P. Boe, F. Kamrath, and M. Höft, "Techniques for the generation of multiple additional transmission zeros in H-plane waveguide filters," *Int. J. Microw. Wireless Technol.*, vol. 12, no. 8, pp. 723–732, Oct. 2020.
[24] L. B. Felsen, M. Mongiardo, and P. Russer, *Electromagnetic Field Computation by Network Methods*. Berlin, Germany: Springer-Verlag, 2009.
[25] Z. Bai, J. Demmel, J. Dongarra, A. Ruhe, and H. van der Vorst, *Templates for the Solution of Algebraic Eigenvalue Problems: A Practical Guide*. Philadelphia, PA, USA: SIAM, 2000.
[26] J. F. Epperson, *An Introduction to Numerical Methods and Analysis*. Hoboken, NJ, USA: Wiley, 2013.
[27] P. Kowalczyk, "Complex root finding algorithm based on delaunay triangulation," *ACM Trans. Math. Softw.*, vol. 41, no. 3, pp. 1–13, Jun. 2015.
[28] J. J. Michalski, "Complex border tracking algorithm for determining of complex zeros and poles and its applications," *IEEE Trans. Microw. Theory Techn.*, vol. 66, no. 12, pp. 5383–5390, Dec. 2018.
[29] V. Mehrmann and H. Voss, "Nonlinear eigenvalue problems: A challenge for modern eigenvalue methods," *GAMM-Mitteilungen*, vol. 27, no. 2, pp. 121–152, Dec. 2004.
[30] W.-J. Beyn, "An integral method for solving nonlinear eigenvalue problems," *Linear Algebra Appl.*, vol. 436, no. 10, pp. 3839–3863, May 2012.
[31] Q. Zhang, T. Guo, B. A. Khan, T. Kodera, and C. Caloz, "Coupling matrix synthesis of nonreciprocal lossless two-port networks using gyrators and inverters," *IEEE Trans. Microw. Theory Techn.*, vol. 63, no. 9, pp. 2782–2792, Sep. 2015.
[32] L. Szydlowski, A. Lamecki, and M. Mrozowski, "Synthesis of coupled-lossy resonator filters," *IEEE Microw. Wireless Compon. Lett.*, vol. 20, no. 7, pp. 366–368, Jul. 2010.
[33] Y. He, G. Wang, L. Sun, and G. Rushingabigwi, "Generalised direct matrix synthesis approach for lossless filters," *IET Microw., Antennas Propag.*, vol. 11, no. 2, pp. 158–164, Jan. 2017.
[34] P. Kozakowski, A. Lamecki, P. Sypek, and M. Mrozowski, "Eigenvalue approach to synthesis of prototype filters with source/load coupling," *IEEE Microw. Wireless Compon. Lett.*, vol. 15, no. 2, pp. 98–100, Feb. 2005.
[35] S. Bastioli and R. V. Snyder, "Nonresonating modes do it better!: Exploiting additional modes in conjunction with operating modes to design better quality filters," *IEEE Microw. Mag.*, vol. 22, no. 1, pp. 20–45, Jan. 2021.
[36] G. Macchiarella, "Generalized coupling coefficient for filters with non-resonant nodes," *IEEE Microw. Wireless Compon. Lett.*, vol. 18, no. 12, pp. 773–775, Dec. 2008.
[37] Q. Zhang, D. L. Sounas, and C. Caloz, "Synthesis of cross-coupled reduced-order dispersive delay structures (DDSs) with arbitrary group delay and controlled magnitude," *IEEE Trans. Microw. Theory Techn.*, vol. 61, no. 3, pp. 1043–1052, Mar. 2013.
[38] R. Gómez-García, J.-M. Muñoz-Ferreras, and D. Psychogiou, "Fully-reconfigurable bandpass filter with static couplings and intrinsic-switching capabilities," in *IEEE MTT-S Int. Microw. Symp. Dig.*, Jun. 2017, pp. 914–917.
[39] L. Balewski *et al.*, "Step on it!: Bringing fullwave finite-element microwave filter design up to speed," *IEEE Microw. Mag.*, vol. 21, no. 3, pp. 34–49, Mar. 2020.

Martyna Mul received the M.Sc.E.E. degree from the Gdańsk University of Technology, Gdańsk, Poland, in 2017.

She is currently with the Department of Microwave and Antenna Engineering, Faculty of Electronics, Telecommunications and Informatics, Gdańsk University of Technology. Her current research interests include computational electromagnetics, microwave filter design, and optimization techniques.

Adam Lamecki (Senior Member, IEEE) received the Ph.D. and D.Sc. degrees in microwave engineering from the Gdańsk University of Technology (GUT), Gdańsk, Poland, in 2007 and 2019, respectively.

In 2007, he cofounded EM Invent, a spin-off company, Gdańsk, which develops an electromagnetic field simulator InventSim, where he currently serves as the CTO. Since 2019, he has been an Associate Professor with the Department of Microwave and Antenna Engineering, GUT. His research interests include surrogate models and their application in the CAD of microwave devices, computational electromagnetics mainly focused on the finite element method, and passive component modeling, design, and optimization techniques.

Roberto Gómez-García (Senior Member, IEEE) was born in Madrid, Spain, in 1977. He received the Dipl.Eng. degree in telecommunication engineering and the Ph.D. degree in electrical and electronic engineering from the Polytechnic University of Madrid, Madrid, in 2001 and 2006, respectively.

Since 2006, he has been an Associate Professor with the Department of Signal Theory and Communications, University of Alcalá, Alcalá de Henares, Spain. His research interests include fixed/tunable high-frequency filters and multiplexers in planar, hybrid, and monolithic microwave-integrated circuit technologies, multifunction circuits and systems, and software-defined radio and radar architectures for telecommunications, remote sensing, and biomedical applications. In these topics, he has published about 120 journal articles and 150 conference papers.

Dr. Gómez-García is also a member of various technical coordinating committees within IEEE MTT and CAS Societies. He was a recipient of the "2016 MTT-S Outstanding Young Engineer Award." He has served/serves as an associate editor and a guest editor for several IEEE, IET, and EuMA journals. He has been an IEEE CAS-S Distinguished Lecturer since 2020.

Michal Mrozowski (Fellow, IEEE) received the M.Sc. degree (Hons.) in telecommunication engineering and the Ph.D. degree (Hons.) in electronic engineering from the Gdańsk University of Technology, Gdańsk, Poland, in 1983 and 1990, respectively.

In 1986, he joined the Department of Electronics, Gdańsk University of Technology, where he is currently a Full Professor, the Head of the Department of Microwave and Antenna Engineering, and the Director of the Doctoral School. He has published one book and over 120 peer-reviewed articles. His research interests include computational electromagnetics, and microwave engineering. His current work is focused on the development of new fast numerical techniques for solving 2-D and 3-D boundary value problems in the time and frequency domains, automated microwave filter design, microwave filter synthesis, reduced-order models for grid-based numerical techniques (e.g., FDTD and FEM), and surrogate model construction.

Dr. Mrozowski is also a member of the MTT-1 and MTT-2 Technical Committees, a Fellow of the Electromagnetics Academy, and a member of the Polish Academy of Sciences. He also serves as a member of the Editorial Board for the PROCEEDINGS OF THE IEEE. He is also a past Vice-Dean for research of the ETI Faculty and the past Chairman of the Polish AES/AP/MTT Chapter. From 2004 to 2005, he has served as an Associate Editor for IEEE MICROWAVE AND WIRELESS COMPONENTS LETTERS.